*Experimental Agriculture* (2024), vol. 60, e25, 1–13
doi:10.1017/S0014479724000206

CAMBRIDGE UNIVERSITY PRESS

RESEARCH ARTICLE

# A non-destructive approach in proximal sensing to assess the performance distribution of SPAD prediction models using hyperspectral analysis in apricot trees

Carmela Riefolo and Laura D'Andrea

Council for Agricultural Research and Economics, Agriculture and Environment Center (CREA-AA), Bari, Italy
**Corresponding author:** Carmela Riefolo; Email: carmela.riefolo@crea.gov.it

(Received 07 March 2024; revised 19 July 2024; accepted 18 September 2024)

**Summary**
SPAD combined with hyperspectral sensors can be an alternative approach to traditional laboratory methods for determining the physiological status of trees. The aim of this work was to assess whether the effectiveness of SPAD predictive models using hyperspectral data might be influenced by where the measurements were carried out. Leaves of apricot trees of two varieties (Farbaly and Farlis) were analysed with SPAD and spectroradiometer, and the data were organized in two different ways: (i) overall dataset (OD), collecting total measurements of trees in each variety; (ii) subset of overall datasets (SOD), collecting the measurements performed on the cardinal points of trees in each variety. Prediction models were built using as regressors: (i) spectral data transformed with Continuum Removal (CR) methodology (CR indices); (ii) vegetation indices (VI) linked to chlorophyll and nitrogen content; (iii) reflectance values associated with chlorophyll content and to wavelengths ranges where (CR) methodology was applied; (iv) reflectance values of full spectrum. The best performances belonged to models using wider ranges of spectrum both in ODs and in SODs. The north cardinal point showed prediction models with the best performances in both varieties. No VI and CR indices showed reliable models. All the reliable prediction models were associated with compounds involved in physiological state and metabolism of leaves in apricot tree.

**Keywords:** chlorophyll content; continuum removal methodology; leaf spectral data; plant physiological state; vegetation index

## Introduction

Apricot (*Prunus armeniaca* L.) is an important fruit crop worldwide, belonging to Rosaceae family. The apricot production was estimated to be about 3,578,412.14 tonnes in the world and 695,632.70 tonnes in Europe, in 2021 (FAOSTAT, 2023). Europe is the second world's apricot producer after Asia (Figure 1). Italy is the fourth world's apricot producer, after Turkey, Iran and Uzbekistan, and it is the largest producer in Europe followed by France, Spain and Greece (Figure 1). In 2021, the apricot annual Italian production was 189 570 tonnes on 17 740 ha of cultivated area, in five Italian Regions: Emilia-Romagna (31%), Campania (21%), Basilicata (20%), Puglia (6%) and Sicilia (5%). In the Mediterranean area, a large part of production is primarily fresh fruit, with a smaller amount destined for processing industry for various products such as dried fruit, fruit cans, jam and juices, ice cream, cheese, etc. (Alvisi, 1997; Chang *et al.*, 2016).

It has been reported that mineral nutrition, particularly nitrogen content (N), plays a key role in plant growth, yield and fruit quality including, firmness, sugar content, phenolic compounds

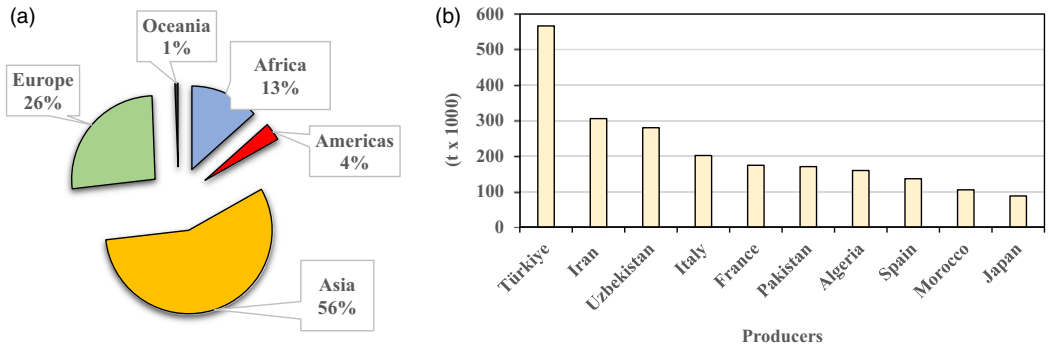


**Figure 1.** Production of apricot by continents (a) and countries (b) in the world (average 1994–2021).

and visual appearance (skin colour) (García-Gomez *et al.*, 2020; Zhebentyayeva *et al.*, 2012; Radi *et al.*, 1997, Radi *et al.*, 2003; Falls and Siegel, 2005; Macheix *et al.*, 2018; Wang *et al.*, 2007; Asma *et al.*, 2007; Dimitrovski and Cvetkovic, 1981). Since nitrogen content in plant was directly associated with chlorophyll synthesis (Boussadia *et al.*, 2010; Kamnev *et al.*, 2008), chlorophyll content in leaves is an indicator of the N status (Li *et al.*, 2009; Shaahan *et al.*, 1999). The proportion of leaf N allocated to the chloroplast is approximately 75% (Hak *et al.*, 1993; Kutik *et al.*, 1995). Leaf N is contained not only in chlorophyll but also in enzymes, vitamins and nucleic acids as well as in proteins. (Carranca *et al.*, 2018; Khasawneh *et al.*, 2021; Khasawneh *et al.*, 2022; Mratinić *et al.*, 2011).

Chlorophyll measurements performed by the SPAD (Soil and Plant Analysis Development) sensor (Minolta Corporation, Ltd., Osaka, Japan) (Minolta Camera, 1989) record chlorophyll values in a non-destructive way by acquiring values of the leaf transmittance at red (650 nm) and infrared (940 nm) wavelengths. The standard method for determining chlorophyll content is very accurate but destructive. (Amirruddin *et al.*, 2020; Wu *et al.*, 2023). Compared with the traditional destructive methods (Porra *et al.*, 1989), SPAD analyses many leaf samples in small amounts of time, space and resources, leading to an exponential increase of its use in the last decade. (Uddling *et al.*, 2007).

Hyperspectral analysis shares the versatility of SPAD, but in a full range of 350–2500 nm. It reads the reflectance with a higher resolution to gather more accurate information (Liu *et al.*, 2020; Tang *et al.*, 2022). These characteristics have been used to assess N content using vegetation indices such as Normalized Difference Nitrogen Index (NDNI) at specific wavelengths (Götze *et al.*, 2010; Osborne *et al.*, 2002) or greater ranges until to the full spectrum between 350–2500 nm (Bruning *et al.*, 2019; Miao *et al.*, 2009). To assess N content, Continuum Removal (CR) methodology was carried out (Kokaly and Clark, 1999) selecting the ranges where absorption peaks were evident along the spectrum (Curran *et al.*, 2001; Huang *et al.*, 2004; Van Der Meer, 2004). While SPAD directly measures chlorophyll at certain wavelengths and this value is correlated with nitrogen content, the spectroradiometer works on the range between 350 and 2500, detecting other signals in the short-wave infrared region (SWIR), between 1400 and 2500 nm, correlated with (a) nitrogen content not of chlorophyll but of other compounds as proteins, enzymes, involved in the plant metabolism; (b) other organic compounds as carbohydrates produced during chlorophyll photosynthesis. Thus, it might help to understand more fully the physiological state of the plant.

Leaf nutrient levels in apricots are non-uniform, showing seasonal variations (Leece and van den Ende, 1975) and dependence upon cultivar (Bojic *et al.*, 1999), rootstock (Rosati *et al.*, 1997, Velemis *et al.*, 1999, Jiménez *et al.*, 2004), interstock (Milosevic 2006, Milosevic and Milosevic 2011) and fertilization (Szücs 1986). It has been reported that the organization or relative amounts

https://doi.org/10.1017/S0014479724000206 Published online by Cambridge University Press

of photosynthetic components differ between sun and shade leaves (Hikosaka and Terashima, 1995; Hoel and Solhaug, 1998). Furthermore, an important component for a higher productivity of quality fruit in an orchard is the design (Javaid *et al.*, 2017) for maximum light interception, and trees should be oriented in North-South direction (Javaid *et al.*, 2017). Other authors (Boissard *et al.*, 1990; Leinonen and Jones, 2004; Paltineanu *et al.*, 2013; Zia *et al.*, 2012, Wang *et al.*, 2024) have studied how leaf orientation and canopy geometry represented by row orientation, row spacing and plant height interact with environmental factors, and the importance of cardinal point in peach, apple and walnut orchards, but not in apricots.

Based on these considerations, in this work an apricot orchard was studied with the following aims:

1) to explore solutions that would make data collection more efficient considering how time-consuming using proximal sensing tools may be. We have studied whether the results of SPAD prediction models might vary depending on the leaf position on the tree. Following studies should evaluate whether some of these positions are more representative of the whole tree, allowing more targeted and efficient data collection. In this preliminary study, the four cardinal points were chosen because they represent easily identifiable standard positions on the apricot tree;
2) to assess plant physiological state in an experimental study where synergy of SPAD and hyperspectral sensor was considered. This is a very preliminary attempt to assess how SPAD prediction models may describe metabolic mechanisms involving other substances, such as sugars, proteins, detected by hyperspectral analysis, during chlorophyll photosynthesis.

Prediction models of SPAD measurements were built using hyperspectral data as auxiliary variables along the entire spectrum between 350 and 2500 nm models or in ranges where absorption peaks were evident along the spectrum (Curran *et al.*, 2001; Huang *et al.*, 2004; Van Der Meer, 2004). These models were built on two types of datasets: (1) with all data collected on tree leaves for each of the two apricot varieties, Farlis and Farbaly; (2) with data grouped according to the four cardinal points on trees of the same apricot varieties.

## Materials and methods

### *Description of site*

The study was conducted on apricot orchard in the Apulia Region (Southern Italy) at latitude 40°53'26" N and longitude 17°5'5" in hilly territory and situated about 20 Km from the Adriatic Sea, in a private farm. The two varieties chosen were Farlis and Farbaly, both were about 8 years old, had a late ripening and a good fruit quality.

The orchard was grown in clay-loam soil and was irrigated using drip system, following the usual agricultural practices of the area. Orchard trees were spaced 3 m within rows and 5.5 m between rows. This study was carried out in July 2021.

### *Sampling design*

Leaves of nine trees of Farlis and Farbaly were analysed in the field. Each tree was divided into 4 cardinal points east, north, south, west. Three leaves were selected on each cardinal point for a total of 108 leaves representing each variety. Three repetitions were measured *in situ* across the leaf with SPAD and after on the same points with Field Spec 4. Finally, the 324 SPAD and spectral data were averaged to get an overall dataset (OD) of 108 measurements that represented each variety. Furthermore, the data of each cardinal point of varieties were elaborated. For this aim,

https://doi.org/10.1017/S0014479724000206 Published online by Cambridge University Press

subsets of the overall dataset (SOD) of 27 SPAD and spectral data represented the cardinal points with each variety.

### SPAD

The SPAD-502 (Minolta Corporation, Ltda., Osaka, Japan) (Minolta, 1989) measured the transmittance of red light (650 nm) and infrared radiation (940 nm) through the leaf giving out a SPAD dimensionless reading as an indicator of the amount of chlorophyll in the leaf tissue according to this equation (Naus *et al.*, 2010) (Eq. 1):

$$SPAD = kxlog\left(\frac{\%trasmission\ 940\ nm}{\%trasmission\ 650\ nm}\right) + C \quad (1)$$

where $k$ is a slope coefficient and $C$ is a confidential offset value.

### Spectral data

#### Hyperspectral analysis

Leaf spectral measurements were performed in the field with ASD Field Spec 4 Portable Spectroradiometer (Analytical Spectral Devices Inc., Boulder, Colorado, USA) on the same points where SPAD analysis was performed. Plant Probe was used to detect a spectral signature in a range of 350–2500 nm. Field Spec 4 provided spectra with 2151 bands having a resolution of 1 nm. The spectral reflectance signatures were averaged over 10 nm to reduce the number of wavelengths from 2151 to 215, smoothing the spectra and keeping down the risk of over-fitting (Shepherd and Walsh, 2002). The calibration was performed by a standard white reference of Plant Probe with a known reflectance of 99% and repeated for each tree, to increase the comparability of measurements.

#### Spectral transformations

Since the aim of this paper was to study the performance of SPAD prediction models, vegetation indices (VI) associated with chlorophyll and nitrogen content were considered. They were Chlorophyll Index (CI), Normalized Pigment Chlorophyll Index (NPCI) associated with chlorophyll content and Normalized Difference Nitrogen Index (NDNI) with nitrogen content (Table 1).

Furthermore, CR methodology was applied on all the ranges along the spectrum of 350–2500 nm showing absorbance peaks (R ranges) to compute $D_{epth}$ (Table 2) as follows (Eq. 2):

$$\boldsymbol{D_{epth}} = 1 - \frac{R_b}{R_e} \quad (2)$$

where Rb is the reflectance at the band bottom and Re is the reflectance on the conjunction line called continuum at the same wavelength of Rb so that no local maximum is higher than 1 (Van Der Meer, 2004). This calculation was performed by ViewSpecPro software (Analytical Spectral Devices Inc., Boulder, Colorado, USA).

### Statistical analysis

#### Prediction and model estimation

Two types of estimation models were applied on ODs and SODs constituted by SPAD values (dependent variable), and spectral data (independent variables or predictors): (i) ordinary least square regression (OLSR) applied on VI and CR indices; (ii) partial least square regression (PLSR) applied on full spectrum of 350–2500 nm (FS) and R ranges. The two apricot varieties were

https://doi.org/10.1017/S0014479724000206 Published online by Cambridge University Press

**Table 1.** Vegetation indices*

| Vegetation index | Acronym | Equation | References |
|---|---|---|---|
| Chlorophyll Index | CI | $(R_{750}–R_{705})/(R_{750}+R_{705})$ | Gitelson and Merzlyak (1994) |
| Normalized Pigment Chlorophyll Index | NPCI | $(R_{680}–R_{430})/(R_{680}+R_{430})$ | Peñuelas *et al.* (1994) |
| Normalized Difference Nitrogen Index | NDNI | $(\log(1/R_{1510}) -\log(1/R_{1680}))/(\log(1/R_{1510}) +\log(1/R_{1680}))$ | Gotze *et al.* (2010) |

*$R_n$ represents the reflectance values and n the wavelength.

**Table 2.** Indices computed with continuum removal methodology*

| Continuum removal index | Minimum wavelength (nm) | Range (nm) | Acronym |
|---|---|---|---|
| $D_{epth710}$ | 710 | 400–820 | R1 |
| $D_{epth1000}$ | 1000 | 820–1110 | R2 |
| $D_{epth1170}$ | 1170 | 1110–1270 | R3 |
| $D_{epth1460}$ | 1460 | 1270–1660 | R4 |
| $D_{epth1840}$ | 1840 | 1660–1870 | R5 |
| $D_{epth1990}$ | 1990 | 1870–2180 | R6 |

*R indicate the ranges along the spectrum of 350–2500 nm showing absorbance peaks.

estimated separately, as well as the cardinal points. The analysis was performed with statistical software package SAS/STAT (release 9.4 SAS ANALYTICS U software).

### *Cross-validation*

Cross-validation was performed as described by Riefolo *et al.* (2020). This procedure was performed on cardinal points subset too: two-third of the subset (18 samples) as calibration set, and the remaining one-third of the samples (9 samples), as validation set. The performance of prediction models was evaluated by means of three statistics: (i) the coefficient of determination in prediction ($R^2$); (ii) root mean square error of prediction (RMSEP); (iii) residual prediction deviation (RPD) (Bellon-Maurel *et al.*, 2010) defined as follows (Eq. 3):

$$\mathbf{RPD} = \boldsymbol{SD}/\boldsymbol{RMSEP} \tag{3}$$

where SD is the standard deviation of the response variable SPAD. It is used to standardize the value of RMSEP with respect to the dispersion of samples enabling to compare the effectiveness of the prediction model as follows: (i) RPD > 2 excellent; (ii) $1.4 \leq \text{RPD} \leq 2$ good; (iii) RPD < 1.4 unreliable (Chang *et al.*, 2001). After cross-validation, analysis of residuals was performed with Shapiro–Wilk and Kolmogorov–Smirnov tests, to evaluate the normality of distribution. The selection of the best model was based on the following criteria: (i) RPD values $\geq 2.0$ with the smaller number of latent variables; (ii) normality of residuals.

### *Analysis of variance*

Analysis of variance of all variables relative to cardinal points was performed to find significative difference among them. The normal distribution of variables was verified by Shapiro-Wilk and Kolmogorov-Smirnov tests to choose the correct analysis of variance (data not shown). Test of Levene verified the homoscedasticity (data not shown). Based on these preliminary tests, four types of analysis of variance with their corresponding post hoc tests were applied (Table 3).

https://doi.org/10.1017/S0014479724000206 Published online by Cambridge University Press

**Table 3.** Types of test and post hoc test for analysis of variance

| Test | Normality | Homoscedasticity | Post hoc test |
|---|---|---|---|
| ANOVA one-way | Yes | Yes | Tukey |
| Welch one-way | Yes | No | Duncan |
| Kruskal-Wallis | No | Yes | Bonferroni |
| Friedman | No | No | Conover |

**Table 4.** Results of ANOVA for some variables concerning cardinal points in Farbaly*

| Indices | East | North | West | South |
|---|---|---|---|---|
| $D_{epth710}$ | $0.89^{a}$ | $0.88^{b}$ | $0.91^{c}$ | $0.89^{abc}$ |
| $D_{epth1000}$ | $0.59^{a}$ | $0.60^{ab}$ | $0.55^{c}$ | $0.56^{ac}$ |
| $D_{epth1170}$ | $0.61^{a}$ | $0.62^{a}$ | $0.57^{b}$ | $0.58^{b}$ |
| $D_{epth1840}$ | $0.81^{a}$ | $0.83^{a}$ | $0.80^{b}$ | $0.77^{c}$ |
| $D_{epth1990}$ | $0.96^{a}$ | $0.95^{ab}$ | $0.97^{ac}$ | $0.93^{a}$ |
| CI | $0.72^{a}$ | $0.68^{b}$ | $0.78^{c}$ | $0.75^{ac}$ |
| NDNI | $0.42^{a}$ | $0.38^{b}$ | $0.44^{a}$ | $0.43^{ab}$ |

*Different letters indicate significant differences ($p < 0.05$) among the cardinal points.

Table 4 shows the results of some VI and CR indices of Farbaly, since SPAD, $D_{epth1460}$ and NPCI index did not show any significative differences.

## Results

A total of 23 SPAD prediction models were fitted for each variety: 8 models for wavelength ranges, full and partial (R ranges) elaborated with Partial Least Square Regression (PLSR) and 9 regarding VI and CR indices elaborated with Ordinary Least Square Regression (OLSR).

### *Analysis of normal distribution*

Table 5 shows the basic statistics of the response variable SPAD for the two varieties in both ODs and SODs. Shapiro-Wilk and Kolmogorov-Smirnov tests were used to assess the normal distribution. When at least one of the two tests was significant at a level probability of 5% ($p < 0.05$), SPAD was transformed in Gaussian ranks by SAS/RANK procedure: the ranks divided by the total number of observations form values in the range 0–1, which were used in subsequent processing. Predictors (VI and CR indices and spectral data) and response variable (SPAD rank transformed) were centred and scaled to have the mean at zero and the variance at 1 and to place both on the same relative position to their variation in the process of prediction model estimation.

### *Prediction models*

#### *Farbaly OD*

Table 6 shows PLSR statistics regarding R ranges. The only value of RPD $\geq$ 1.4 belonged to R1R6 range with 9 factors, (highest $R^2$ 0.623 and lowest RMSEP 0.610) (Figure 2). No VI and CR indices showed a RPD value $\geq$ 1.4 with an explained variance that never exceeded 10% (data not shown).

#### *Farbaly subsets*

Table 7 shows PLSR statistics of SODs in descending order of RPD values until the last good effective model. Although the greatest value of RPD belonged to the R1R6 range in the east SOD (10.657), that represented by the R3 range of the same SOD was chosen as the best model (2.160)

https://doi.org/10.1017/S0014479724000206 Published online by Cambridge University Press

**Table 5.** Basic statistics of response variable SPAD for the two apricot varieties

| | Farbaly | | | | | Farlis | | | | |
|---|---|---|---|---|---|---|---|---|---|---|
| Parameters | Overall | East | North | West | South | Overall | East | North | West | South |
| Mean | 36.0 | 36.3 | 35.8 | 36.4 | 35.4 | 37.0 | 37.6 | 37.0 | 37.0 | 36.4 |
| Standard Deviation | 1.51 | 0.96 | 1.73 | 1.32 | 1.75 | 1.49 | 1.57 | 1.42 | 1.45 | 1.34 |
| Range | 9.24 | 4.08 | 5.60 | 5.76 | 7.20 | 6.62 | 5.42 | 5.54 | 5.16 | 4.46 |
| Skewness | −0.74 | 0.88 | −0.19 | 0.25 | −1.41 | 0.32 | 0.85 | 0.34 | −0.39 | 0.12 |
| Kurtosis | 1.61 | 0.70 | −1.09 | 0.01 | 2.02 | −0.18 | −0.27 | −0.46 | −0.47 | −1.22 |
| Shapiro-Wilk ($W^*$) | 0.96 | 0.94 | 0.94 | 0.97 | 0.86 | 0.98 | 0.89 | 0.96 | 0.95 | 0.95 |
| P value | 0.00 | 0.16 | 0.11 | 0.67 | 0.00 | 0.13 | 0.01 | 0.40 | 0.21 | 0.21 |
| Kolmogorov-Smirnov ($D^\dagger$) | 0.08 | 0.14 | 0.14 | 0.12 | 0.16 | 0.06 | 0.20 | 0.15 | 0.13 | 0.13 |
| P value | 0.13 | >0.15 | >0.15 | >0.15 | 0.07 | >0.15 | <0.01 | 0.12 | >0.15 | >0.15 |

*Mathematic factor computed by Shapiro-Wilk test.
†Mathematic factor computed by Kolmogorov-Smirnov test.

**Table 6.** Statistics of PLSR and analysis of residuals of SPAD for the two apricot varieties (OD)

| Varieties | Input data | Factor | $R^2$ | RMSEP | RPD | $W^*$ | P value | $D^\dagger$ | P value |
|---|---|---|---|---|---|---|---|---|---|
| Farbaly | Full spectrum | 1 | 0.06 | 0.96 | 1.03 | 1.00 | 1.00 | 0.03 | >0.15 |
| | R1 | 5 | 0.21 | 0.89 | 1.12 | 0.98 | 0.14 | 0.07 | >0.15 |
| | R2 | 5 | 0.29 | 0.84 | 1.18 | 0.99 | 0.55 | 0.06 | >0.15 |
| | R3 | 4 | 0.24 | 0.87 | 1.14 | 0.99 | 0.52 | 0.06 | >0.15 |
| | R4 | 1 | 0.06 | 0.97 | 1.02 | 1.00 | 1.00 | 0.03 | >0.15 |
| | R5 | 5 | 0.29 | 0.84 | 1.18 | 0.99 | 0.87 | 0.04 | >0.15 |
| | R6 | 0 | 0.00 | 0.99 | 1.00 | 1.00 | 1.00 | 0.02 | >0.15 |
| | R1R6 | 9 | 0.62 | 0.61 | 1.62 | 0.98 | 0.07 | 0.05 | >0.15 |
| Farlis | Full spectrum | 15 | 0.89 | 0.50 | 2.95 | 0.99 | 0.96 | 0.04 | >0.15 |
| | R1 | 5 | 0.34 | 1.22 | 1.22 | 0.98 | 0.07 | 0.08 | 0.05 |
| | R2 | 9 | 0.46 | 1.10 | 1.35 | 0.99 | 0.68 | 0.05 | >0.15 |
| | R3 | 1 | 0.21 | 1.33 | 1.12 | 0.99 | 0.71 | 0.05 | >0.15 |
| | R4 | 8 | 0.49 | 1.07 | 1.39 | 0.99 | 0.62 | 0.07 | >0.15 |
| | R5 | 1 | 0.09 | 1.42 | 1.05 | 0.99 | 0.38 | 0.07 | >0.15 |
| | R6 | 1 | 0.08 | 1.43 | 1.04 | 0.99 | 0.39 | 0.05 | >0.15 |
| | R1R6 | 1 | 0.21 | 1.33 | 1.12 | 0.99 | 0.45 | 0.06 | >0.15 |

*Mathematic factor computed by Shapiro-Wilk test.
†Mathematic factor computed by Kolmogorov-Smirnov test.

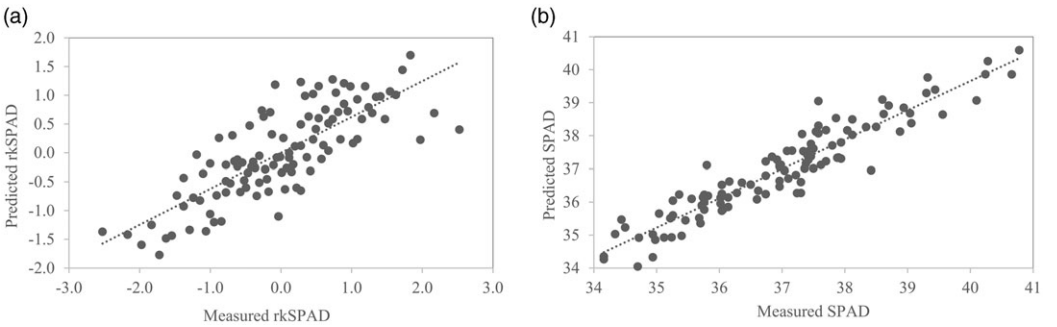


**Figure 2.** Predicted vs measured SPAD values in the R1R6 model for Farbaly (a) and in the FS model for Farlis (b).

https://doi.org/10.1017/S0014479724000206 Published online by Cambridge University Press

**Table 7.** The better models of the two apricot varieties concerning the cardinal points subsets (SOD) with analysis of residuals

| Varieties | SOD | Input data | Factor | $R^2$ | RMSEP | RPD | W* | P value | D† | P value | SD |
|---|---|---|---|---|---|---|---|---|---|---|---|
| Farbaly | East | R1R6 | 11 | 0.99 | 0.09 | 10.7 | 0.97 | 0.54 | 0.10 | >0.15 | 0.96 |
| | North | FS | 10 | 1.00 | 0.19 | 8.94 | 0.97 | 0.72 | 0.09 | >0.15 | 1.73 |
| | North | R2 | 11 | 0.97 | 0.28 | 6.12 | 0.97 | 0.52 | 0.10 | >0.15 | 1.73 |
| | South | FS | 6 | 0.96 | 0.19 | 4.98 | 0.99 | 0.97 | 0.11 | >0.15 | 0.97 |
| | East | FS | 6 | 0.95 | 0.22 | 4.42 | 0.96 | 0.28 | 0.11 | >0.15 | 0.96 |
| | South | R1R6 | 6 | 0.94 | 0.25 | 3.91 | 0.98 | 0.82 | 0.07 | >0.15 | 0.97 |
| | East | R6 | 7 | 0.85 | 0.37 | 2.58 | 0.96 | 0.35 | 0.12 | >0.15 | 0.96 |
| | East | R1 | 8 | 0.83 | 0.41 | 2.37 | 0.98 | 0.79 | 0.13 | >0.15 | 0.96 |
| | West | R2 | 7 | 0.83 | 0.56 | 2.35 | 0.94 | 0.13 | 0.16 | 0.07 | 1.32 |
| | **East** | **R3** | **5** | **0.79** | **0.45** | **2.16** | **0.95** | **0.27** | **0.10** | **>0.15** | **0.96** |
| | South | R1 | 6 | 0.78 | 0.47 | 2.08 | 0.96 | 0.44 | 0.14 | >0.15 | 0.97 |
| Farlis | North | FS | 9 | 0.99 | 0.14 | 10.4 | 0.98 | 0.78 | 0.11 | >0.15 | 1.42 |
| | North | R1R6 | 7 | 0.97 | 0.26 | 5.46 | 0.97 | 0.69 | 0.11 | >0.15 | 1.42 |
| | North | R2 | 11 | 0.97 | 0.28 | 5.05 | 0.95 | 0.52 | 0.09 | >0.15 | 1.42 |
| | North | R4 | 9 | 0.94 | 0.34 | 4.19 | 0.97 | 0.62 | 0.12 | >0.15 | 1.42 |
| | East | FS | 7 | 0.94 | 0.24 | 4.04 | 0.97 | 0.68 | 0.08 | >0.15 | 0.97 |
| | West | R2 | 8 | 0.84 | 0.59 | 2.45 | 0.97 | 0.59 | 0.11 | >0.15 | 1.45 |
| | East | R4 | 7 | 0.83 | 0.40 | 2.40 | 0.96 | 0.44 | 0.15 | 0.10 | 0.97 |
| | West | FS | 5 | 0.82 | 0.63 | 2.29 | 0.94 | 0.10 | 0.20 | <0.01 | 1.45 |
| | **East** | **R1** | **5** | **0.81** | **0.43** | **2.28** | **0.97** | **0.74** | **0.09** | **>0.15** | **0.97** |
| | West | R1 | 8 | 0.81 | 0.64 | 2.25 | 0.97 | 0.49 | 0.12 | >0.15 | 1.45 |

In bold the models chosen for each variety.
*Mathematic factor computed by Shapiro-Wilk test.
†Mathematic factor computed by Kolmogorov-Smirnov test.

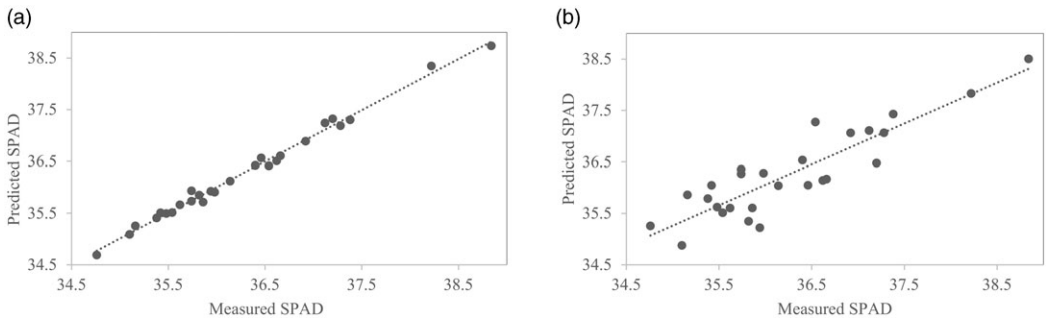


**Figure 3.** Predicted vs measured SPAD values in the R1R6 model (a) and in the R3 model for SOD east of Farbaly (b).

(Figure 3). It, among the models with an excellent RPD value, shows the lowest number of factors. Ten models have an excellent RPD value and a normal distribution of residuals (Table 7) and eight a good one (data not shown). Considering the models with RPD $\geq$ 1.4, the north SOD is represented six times while the west one only once (data not shown).

No VI and CR indices show a RPD value $\geq$ 1.4 both with an explained variance that never exceeds 50% (data not shown). The highest value of explained variance belongs to $D_{epth1000}$ (49,90%) with a RMSEP of 0,696 and a RPD of 1.386, followed by $D_{epth1460}$ (41,30%) with a RMSEP of 0,754 and a RPD of 1.280 in east SOD.

https://doi.org/10.1017/S0014479724000206 Published online by Cambridge University Press

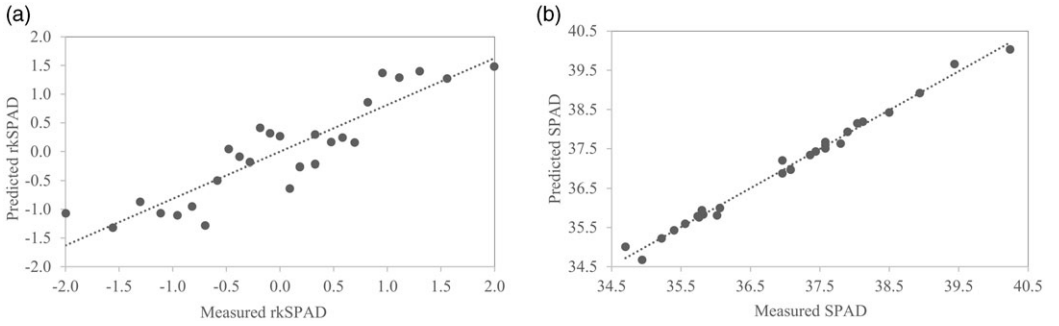


**Figure 4.** Predicted vs measured SPAD values in the R1 model for SOD east (a) and in the FS model for SOD north of Farlis (b).

*Farlis OD*

Table 6 shows PLSR statistics regarding R ranges. The only value of RPD $\geq$ 2.0 belonged FS range, with 15 factors (highest $R^2$ 0.886 and lowest RMSEP 0.504) (Figure 2) while the other ranges never exceeded the 1.4 value. No VI and CR indices show a RPD value $\geq$ 1.4 both in OD with an explained variance that never exceeded 12% (data not shown).

*Farlis subsets*

Table 7 shows PLSR statistics of SODs in descending order of RPD values until the last good effective model. Although the greatest value of RPD belongs to the FS range in the north SOD (10.394), that represented by the R1 range of the east SOD was chosen as the best model (2.276), since it showed the lowest number of factors and a normal distribution of residuals (Figure 4). Nine models had an excellent RPD value and a normal distribution of residuals (Table 7), six a good one (data not shown). Since the west SOD model departed by the normal distribution, it is excluded by the effective models. Considering the models with RPD $\geq$ 1.4, the north SOD is represented six times, while the south one twice (data not shown).

No VI and CR indices show a RPD value $\geq$ 1.4 both with an explained variance that is around 15% (data not shown). The highest value of explained variance belongs to NDNI (15.44%) with a RMSEP of 1.470 and a RPD of 1.067, in east SOD, followed by NPCI (15.23%) with a RMSEP of 1.260 and a RPD of 1.062 in south SOD.

## Discussion

The models based on the wider ranges of spectrum, FS and R1R6, were the best ones both in Farlis and Farbaly ODs (Table 6). Considering the SODs results, the cardinal point east in Farbaly and the north one in Farlis showed the highest number of excellent models (Table 7). However, in Farbaly north SOD showed the highest number of models with RPD $\geq$ 1.4 (data not shown). These results were consistent with those of the ANOVA for Farbaly, since the north cardinal point showed the highest number of significative differences, 14, followed by the west one and as the lowest the south one (Table 4). Farlis showed a significative difference in CI index only between north and south cardinal point at a level of 1% (data not shown). The results suggested the possibility that metabolic behaviour could vary within the plant, even according to cardinal points and the importance of row direction in orchard design as reported by Javaid *et al.* (2017).

Considering the R ranges corresponding to the absorbance peaks where $D_{epths}$ were calculated (Table 2), the R1 and R2 ranges included the wavelengths at which SPAD and the spectroradiometer both worked. From R3 onward, only the spectroradiometer was working.

https://doi.org/10.1017/S0014479724000206 Published online by Cambridge University Press

They have been associated with physiological characteristics of the plant based on previous studies. R1 (400–820 nm) corresponded to the absorbance range of chlorophyll while R2 (820–1110 nm) was associated with leaf structure (Bauer, 1985; Knipling, 1970; Peñuelas *et al.*, 1993). The results showed excellent RPD for these two models to the north and east in both Farbaly and Farlis, and this was attributed to the fact that R1 and R2 ranges included SPAD wavelengths (650 and 930 nm). R3 range was associated with leaf water content (Clevers *et al.*, 2010; González-Fernández *et al.*, 2015). It became interesting to note that although there was no longer the overlap with the wavelengths where SPAD worked, for R3 the RPD value was still reliable in both Farbaly to the east (2.16) (Table 7) and Farlis to the north (1.88, not shown in Table 7). This could have been caused by the relationship between leaf structure, characterizing R2 where SPAD also worked, and R3 characterizing leaf water content. From the R3 range onward, the prediction models with the highest RPD no longer belonged to the same cardinal points in Farbaly and Farlis. Farbaly showed a good value of RPD for R6 model, whereas Farlis showed an excellent RPD value for R4 model. The ranges corresponding to R4 and R6, shared an association with organic compounds, involving stretching and bending deformations of O-H link as in the carbohydrates, over all in starch that represents plant energy reserve (Fourty *et al.*, 1996). Therefore, these prediction models might be associated with photosynthetic activity. But whereas the R4 model would refer only to carbohydrates, the R6 one would also be associated with the presence of protein (Ecarnot *et al.*, 2013; Fourty *et al.*, 1996). Both varieties showed that the R4 and R6 models were mutually exclusive: when one model is reliable, the other is not. RPD value for R5 model associated with cellulose (Fourty *et al.*, 1996; Shenk *et al.*, 2001) forming the structural basis of the tree (roots, stems and leaves), resulted good only for Farbaly. This could confirm that the prediction models of SPAD produced are associated with compounds concerning the metabolic activity of leaf and not of tree structure. It is noteworthy that these compounds have a chemical affinity with water, associated with the ranges showing good predictive models at the north cardinal point. So, these results should confirm that the row direction in orchard design gets maximum light interception in trees as reported by Javaid *et al.* (2017).

## Conclusion

In this paper, the variation of physiological response on different cardinal points of apricot trees was studied. This study is in addition to others with similar purposes carried out in the past on other types of orchards. The choice to assess the efficiency of SPAD prediction models on cardinal points showed the best results for the north one. VI and CR indices did not produce reliable predictive models even if their analysis of variance showed a greater number of significative differences for north. Considering both the OD and the subsets of cardinal points, models referring to the widest ranges of wavelengths showed the best performance. When the wavelengths ranges where SPAD worked no longer overlapped that of the hyperspectral sensor, the cardinal points of the best predictive models were not the same in the two varieties. These preliminary results, although agreeing with those of other studies, should be confirmed using more measurements taken on each cardinal point. They suggest the possibility of identifying plant points more suitable for producing reliable prediction models of SPAD that, involving many aspects of the leaf metabolic activity thanks to hyperspectral analysis, enable to assess plant physiological state.

**Author contributions.** CR contributed to methodology, software, validation, formal analysis, writing – original draft preparation, visualization. CR and LD contributed to conceptualization, investigation, data curation, writing – review and editing. LD contributed to resources, supervision, project administration and funding acquisition.

**Funding statement.** This research was carried out in the framework of the project 'TAGs – Technological and business innovation services to stimulate the local Agro-Food ecosystems and to support a cross-border collaboration among local

action Groups', a project co-funded by European Union, European Regional Development Funds (E.R.D.F.) and by National Funds of Greece and Italy, Interreg V-A Greece-Italy Programme 2014–2020 (MIS CODE: 5 003 507).

**Competing interests.** None.

## References

**Alvisi, F.** (1997) Situazione e prospettive della produzione e commercializzazione delle albicocche nel mediterraneo. *Italus Hortus* **4**, 7–11.

**Amirruddin, A.D., Muharam, F.M., Ismail, M.H., Ismail, M.F., Tan, N.P. and Karam, D.S.** (2020) Hyperspectral remote sensing for assessment of chlorophyll sufficiency levels in mature oil palm (*Elaeis guineensis*) based on frond numbers: analysis of decision tree and random forest. *Computers and Electronics in Agriculture* **169**, 105221.

**Asma, B.M., Colak, S., Akca, Y. and Genc, C.** (2007) Effect of fertiliser rate on the growth, yield and fruit characteristics of dried apricot (cv. *Hacihaliloglu*). *Asian Journal of Plant Science* **6**, 294–297.

**Bauer, M.E.** (1985) Spectral inputs to crop identification and condition assessment. *Proceedings of the Institute of Electrical and Electronics Engineers* **73**, 1071–1085.

**Bellon-Maurel, V., Fernandez-Ahumada, E., Roger, B.P.J.M. and McBratney, A.** (2010) Critical review of chemometric indicators commonly used for assessing the quality of the prediction of soil attributes by NIR spectroscopy. *Trends in Analytical Chemistry* **29**, 1073–1081.

**Boissard, P., Guyot, G. and Jackson, R.D.** (1990) Factors affecting the radiative surface temperature of vegetative canopy. In Steven, M.D., Clark, J.A. (eds.), *Application of Remote Sensing in Agriculture*. London: Butterworths, pp. 45–72.

**Bojic, M., Milosevic, T. and Rakocevic, L.** (1999) Macro and microelement content of leaves of the apricot cv. *Roxana* grafted on two rootstocks. *Acta Horticulturae* **488**, 543–546.

**Boussadia, O., Steppe, K., Zgallai, H., Ben El Hadj, S., Braham, M., Lemeur, R. and Van Labeke, M.C.** (2010) Effects of nitrogen deficiency on leaf photosynthesis, carbohydrate status and biomass production in two olive cultivars '*Meski*' and '*Koroneiki*'. *Scientia Horticulturae* **123**, 336–342.

**Bruning, B., Liu, H., Brien, C., Berger, B., Lewis, M. and Garnett, T.** (2019) The development of hyperspectral distribution maps to predict the content and distribution of nitrogen and water in wheat (*Triticum aestivum*). *Frontiers in Plant Science* **10**, 1380.

**Carranca, C., Brunetto, G. and Tagliavini, M.** (2018) Nitrogen nutrition of fruit trees to reconcile productivity and environmental concerns. *Plants* **7**, 4.

**Chang, C.W., Laird, D.A., Mausbach, M.J. and Hurburgh, C.R.** (2001) Near-infrared reflectance spectroscopy–principal components regression analyses of soil properties. *Soil Science Society of America Journal* **65**, 480–490.

**Chang, S.K., Alasalvar, C. and Shahidi, F.** (2016) Review of dried fruits: phytochemicals, antioxidant efficacies, and health benefits. *Journal of Functional Foods* **21**, 113–132.

**Clevers, J.G.P.W., Kooistra, L. and Schaepman, M.E.** (2010) Estimating canopy water content using hyperspectral remote sensing data. *International Journal of Applied Earth Observation and Geoinformation* **12**, 119–125.

**Curran, P.J., Dungan, J.L. and Peterson, D.L.** (2001) Estimating the foliar biochemical concentration of leaves with reflectance spectrometry, testing the Kokaly and Clark methodologies. *Remote Sensing of Environment* **76**, 349–359.

**Dimitrovski, T. and Cvetkovic, D.** (1981) The effect of NPK on growth, yield and quality of the apricot fruit. *Acta Horticulturae* **85**, 481–489.

**Ecarnot, M., Compan, F. and Roumet, P.** (2013) Assessing leaf nitrogen content and leaf mass per unit area of wheat in the field throughout plant cycle with a portable spectrometer. *Field Crops Research* **140**, 44–50.

**FAOSTAT** (2023) FAOSTAT. Available at http://faostat.fao.org (accessed 26 September 2024).

**Falls, J. and Siegel, S.** (2005) Fertilizers. In Poole, C., Townshend, A., Worsfold, P. (eds.), *Encyclopedia of Analytical Science*, 2nd Edn. Amsterdam: Elsevier, pp. 1–8.

**Fourty, T., Baret, F., Jacquemoud, S., Schmuck, G. and Verdebout, J.** (1996) Leaf optical properties with explicit description of its biochemical composition: direct and inverse problems. *Remote Sensing of Environment* **56**, 104–117.

**García-Gomez, B., Ruiz, D., Salazar, J.A., Rubio, M., Martínez-García, P. and Martínez-Gomez, P.** (2020) Analysis of metabolites and gene expression changes relative to apricot (*Prunus armeniaca* L.) fruit quality during development and ripening. *Frontiers in Plant Science* **11**, 1269.

**Gitelson, A. and Merzlyak, M.N.** (1994) Quantitative estimation of chlorophyll-a using reflectance spectra: experiments with autumn chestnut and maple leaves. *Journal of Photochemistry and Photobiology B: Biology* **22**, 247–252.

**González-Fernández, A.B., Rodríguez-Pérez, J.R., Marabel, M. and Álvarez-Taboada, F.** (2015) Spectroscopic estimation of leaf water content in commercial vineyards using continuum removal and partial least squares regression. *Scientia Horticulturae* **188**, 15–22.

**Götze, C., Jung, A., Merbach, I., Wennrich, R. and Gläßer, C.** (2010) Spectrometric analyses in comparison to the physiological condition of heavy metal stressed floodplain vegetation in a standardised experiment. *Central European Journal of Geosciences* **2**, 132–137.

**Hak, R., Rinderle-Zimmer, U., Lichtenthaler, H.K. and Natr, L.** (1993) Chlorophyll a fuorescence signatures of nitrogen defcient barley leaves. *Photosynthetica* **28**, 151–159.

**Hikosaka, K. and Terashima, I.** (1995) A model of the acclimation of photosynthesis in the leaves of C3 plants to sun and shade with respect to nitrogen use. *Plant Cell and Environment* **18**, 605–606.

**Hoel, B.O. and Solhaug, K.A.** (1998) Effect of irradiance on chlorophyll estimation with the Minolta SPAD-502 leaf chlorophyll meter. *Annals of Botany* **82**, 389–392.

**Huang, Z., Turner, B.J., Dury, S.J., Wallis, I.R. and Foley, W.J.** (2004) Estimating foliage nitrogen concentration from HYMAP data using continuum removal analysis. *Remote Sensing of Environment* **93**, 18–29.

**Javaid, K., Qureshi, S.N., Masoodi, L., Sharma, P., Fatima, N. and Saleem, I.** (2017) Orchard designing in fruit crops. *Journal of Pharmacognosy and Phytochemistry* **6**, 1081–1091.

**Jiménez, S., Garín, A., Gogorcena, Y., Betrán, A.J. and Moreno, A.M.** (2004) Flower and foliar analysis for prognosis of sweet cherry nutrition: influence of different rootstocks. *Journal of Plant Nutrition* **27**, 701–712.

**Leinonen, I. and Jones, H.G.** (2004) Combining thermal and visible imagery for estimating canopy temperature and identifying plant stress. *Journal of Experimental Botany* **55**, 1423–1431.

**Kamnev, A.A., Sadovnikova, Y.N. and Antonyuk, L.P.** (2008) Effects of nitrogen deficiency and wheat lectin on the composition and structure of some biopolymers of azospirillum brasilense Sp245. *Microbiology* **77**, 240–242.

**Khasawneh, A., Alsmairat, N., Othman, Y., Ayad, J., Al-Hajaj, H. and Qrunfleh, I.** (2022) Controlled-release nitrogen fertilizers for improving yield and fruit quality of young apricot trees. *Scientia Horticulturae* **303**, 111233.

**Khasawneh, A., Alsmairat, N., Othman, Y., Ayad, J., Al-Qudah, T. and Leskovar, D.** (2021) Influence of nitrogen source on physiology, yield and fruit quality of young apricot trees. *Journal of Plant Nutrition* **44**, 2597–2608.

**Knipling, E.B.** (1970) Physical and physiological basis for the reflectance of visible and nearinfrared radiation from vegetation. *Remote Sensing of Environment* **1**, 155–159.

**Kokaly, R.F. and Clark, R.N.** (1999) Spectroscopic determination of leaf biochemistry using band-depth analysis of absorption features and stepwise multiple linear regression. *Remote Sensing of Environment* **67**, 267–287.

**Kutik, J., Nátr, L., Demmers-Derks, H.H. and Lawlor, D.W.** (1995) Chloroplast ultrastructure of sugar beet (Beta vulgaris L.) cultivated in normal and elevated CO2 concentrations with two contrasted nitrogen supplies. *Journal of Experimental Botany* **46**, 1797–1802.

**Leece, D.R. and van den Ende, B.** (1975) Diagnostic leaf analysis for stone fruit. 6. Apricot. *Australian Journal of Experimental Agriculture and Animal Husbandry* **15**, 123–128.

**Li, J.W., Yang, J.P., Fei, P.P., Song, J.L., Li, D.S., Ge, C.S. and Chen, W.Y.** (2009) Responses of rice leaf thickness, SPAD readings and chlorophyll a/b ratios to different nitrogen supply rates in paddy field. *Field Crops Research* **114**, 0–432.

**Liu, W.W., Li, M.J., Zhang, M.Y., Wang, D.A., Guo, Z.L., Long, S.Y., Yang, S., Wang, H.N., Li, W., Hu, Y.K., Wei, Y. and Xiao, H.** (2020) Estimating leaf mercury content in Phragmites australis based on leaf hyperspectral reflectance. *Ecosystem Health Sustainability* **6**, 1726211.

**Macheix, J.J., Fleuriet, A. and Billot, J.** (2018) *Fruit Phenolics*, Boca Raton: CRC Press.

**Miao, Y., Mulla, D.J., Randall, G.W., Vetsch, J.A. and Vintila, R.** (2009) Combining chlorophyll meter readings and high spatial resolution remote sensing images for in-season site specific nitrogen management of corn. *Precision Agriculture* **10**, 45–62.

**Milosevic, T. and Milosevic, N.** (2011) Seasonal changes in micronutrients concentrations in leaves of apricot trees influenced by different interstocks. *Agrochimica* **15**, 1–14.

**Milosevic, T.** (2006) Effect of interstock on seasonal changes in microelement concentrations in apricot leaf. *Acta Horticulturae* **701**, 719–722.

**Minolta Camera, CO.** (1989) *Manual for Chlorophyll SPAD 502*. Osaka: Minolta Radiometric Instruments Divisions.

**Mratinić, E., Popovski, B., Milošević, T. and Popovska, M.** (2011) Evaluation of apricot fruit quality and correlations between physical and chemical attributes. *Czech Journal of Food Science* **29**, 161–170.

**Naus, J., Prokopova, J., Rebicek, J. and Spundova, M.** (2010) Spad chlorophyll meter reading can be pronouncedly affected by chloroplast movement. *Photosynthesis Research* **105**, 265–271.

**Osborne, S.L., Schepers, J.S., Francis, D.D. and Schlemmer, M.R.** (2002) Use of spectral radiance to estimate in-season biomass and grain yield in nitrogen-and water-stressed corn. *Crop Science* **42**, 165–171.

**Paltineanu, C., Septar, L. and Moale, C.** (2013) Crop water stress in peach orchards and relationships with soil moisture content in a chernozem of Dobrogea. *Journal of Irrigation and Drainage Engineering* **139**, 20–25.

**Peñuelas, J., Gamon, J., Fredeen, A., Merino, J. and Field, C.** (1994) Reflectance indices associated with physiological changes in nitrogen-and water-limited sunflower leaves. *Remote Sensing of Environment* **48**, 135–146.

**Peñuelas, J., Filella, I., Biel, C., Serrano, L. and Save, R.** (1993) The reflectance at the 950–970 nm region as an indicator of plant water status. *International Journal of Remote Sensing* **14**, 1887–1905.

**Porra, R.J., Thompson, W.A. and Kriedemann, P.E.** (1989) Determination of accurate extinction coefficients and simultaneous equations for assaying chlorophylls *a* and *b* extracted with four different solvents: verification of the concentration of chlorophyll standards by atomic absorption spectroscopy. *Biochimica and Biophysica Acta-Bioenergetics* **975**, 384–394.

**Radi, M., Mahrouz, M., Jaouad, A. and Amiot, M.** (2003) Influence of mineral fertilization (NPK) on the quality of apricot fruit (cv. *Canino*); the effect of the mode of nitrogen supply. *Agronomie*, **23**, 737–745.

**Radi, M., Mahrouz, M., Jaouad, A., Tacchini, M., Hugues, M. and Amiot, M.J.** (1997) Phenolic composition, browning susceptibility and carotenoid content on several apricot cultivars at maturity. *HortScience* **32**, 1087–1091.

**Riefolo, C., Castrignanò, A., Colombo, C., Conforti, M., Ruggieri, S., Vitti, C. and Buttafuoco, G.** (2020) Investigation of soil surface organic and inorganic carbon contents in a low-intensity farming system using laboratory visible and near-infrared spectroscopy. *Archives of Agronomy and Soil Science* **66**, 1436–1448.

**Rosati, A., DeJong, T.M. and Southwick, S.M.** (1997) Comparison of leaf mineral content, carbon assimilation and stem water potential of two apricot (*Prunus armeniaca*) cultivars grafted on '*Citation*' and '*Marianna 2624*' rootstock. *Acta Horticulturae* **451**, 263–268.

**Shaahan, M.M., El-Sayed, A.A. and Abou El-Nour, E.A.A.** (1999) Predicting nitrogen, magnesium and iron nutritional status in some perennial crops using a portable chlorophyll meter. *Scientia Horticulturae* **82**, 339–348.

**Shenk, J.S., Workman, J. and Westerhaus, M.O.** (2001) Application of NIR spectroscopy to agricultural products. In Burns, D.A., Ciurczak, E.D. (eds.), *Handbook of NearInfrared Analysis (Practical Spectroscopy Series)*. New York, NY: CRC Press, pp. 419–474.

**Shepherd, K.D. and Walsh, M.G.** (2002) Development of reflectance spectral libraries for characterization of soil properties. *Soil Science Society of America Journal* **66**, 988–998.

**Szücs, E.** (1986) Effects of fertilization on nutrient supply, yield, growth and frost hardiness of apricot trees. *Acta Horticulturae* **192**, 137–142.

**Tang, X.Y., Dou, Z.G., Cui, L.J., Liu, Z.J., Gao, C.J., Wang, J.J., Li, J., Lei, Y.R., Zhao, X.S., Zhai, X.J. and Li, W.** (2022) Hyperspectral prediction of mangrove leaf stoichiometries in different restoration areas based on machine learning models. *Journal of Applied Remote Sensing* **16**, 034525.

**Uddling, J., Gelang-Alfredsson, J., Piikki, K. and Pleijel, H.** (2007) Evaluating the relationship between leaf chlorophyll concentration and SPAD-502 chlorophyll meter readings. *Photosyntesis Research* **91**, 37–46.

**Van Der Meer, F.** (2004) Analysis of spectral absorption features in hyperspectral imagery. *International Journal of Applied Earth Observation and Geoinformation* **5**, 55–68.

**Velemis, D., Almaliotis, D., Bladenopoulou, S. and Karayiannis, I.** (1999) Growth and nutritional status of twelve apricot varieties grafted on two rootstocks. *Acta Horticulturae* **488**, 489–494.

**Wang, F., Wang, H. and Wang, G.** (2007) Photosynthetic responses of apricot (*Prunus armeniaca* L.) to photosynthetic photon flux density, leaf temperature, and CO2 concentration. *Photosynthetica* **45**, 59–64.

**Wang, R., Tuerxun, N. and Zheng, J.** (2024) Improved estimation of SPAD values in walnut leaves by combining spectral, texture, and structural information from UAV-based multispectral image. *Scientia Horticulturae* **328**, 112940.

**Wu, Q., Zhang, Y.P., Zhao, Z.W., Xie, M. and Hou, D.Y.** (2023) Estimation of relative chlorophyll content in spring wheat based on multi-temporal UAV remote sensing. *Agronomy* **13**, 211.

**Zhebentyayeva, T., Ledbetter, C.A., Burgos, L. and Ll´acer, G.** (2012) Apricots. In Badenes, M. L., Byrne, P.H. (eds.), *Handbook of Plant Breeding. Volume 8. Fruit Breeding*. New York: Springer, pp. 875–890.

**Zia, S., Wenyong, D., Spreer, W., Spohrer, K., Xiongkui, H. and Müller, J.** (2012) Assessing crop water stress of winter wheat by thermography under different irrigation regimes in North China Plain. *International Journal of Agricultural and Biological Engineering* **5**, 24–34.

**Cite this article:** Riefolo C and D'Andrea L. A non-destructive approach in proximal sensing to assess the performance distribution of SPAD prediction models using hyperspectral analysis in apricot trees. *Experimental Agriculture*. https://doi.org/10.1017/S0014479724000206